Pergamon

Geochimica et Cosmochimica Acta, Vol. 68, No. 15, pp. 3205–3216, 2004

0016-7037/04 $30.00 + .00

doi:10.1016/j.gca.2004.03.028

Analysis of long-term bacterial vs. chemical Fe(III) oxide reduction kinetics

ERIC E. RODEN*

Department of Biological Sciences, The University of Alabama, Tuscaloosa, AL 35487-0206, USA

(*Received July* 1, 2003; *accepted in revised form March* 30, 2004)

Abstract—Data from studies of dissimilatory bacterial (10^8 cells mL^{-1} of *Shewanella putrefaciens* strain CN32, pH 6.8) and ascorbate (10 mM, pH 3.0) reduction of two synthetic Fe(III) oxide coated sands and three natural Fe(III) oxide-bearing subsurface materials (all at ca. 10 mmol Fe(III) L^{-1}) were analyzed in relation to a generalized rate law for mineral dissolution ($J_t/m_0 = k'(m/m_0)^{\gamma}$, where J_t is the rate of dissolution and/or reduction at time t, m_0 is the initial mass of oxide, and m/m_0 is the unreduced or undissolved mineral fraction) in order to evaluate changes in the apparent reactivity of Fe(III) oxides during long-term biological vs. chemical reduction. The natural Fe(III) oxide assemblages demonstrated larger changes in reactivity (higher γ values in the generalized rate law) compared to the synthetic oxides during long-term abiotic reductive dissolution. No such relationship was evident in the bacterial reduction experiments, in which temporal changes in the apparent reactivity of the natural and synthetic oxides were far greater (5–10 fold higher γ values) than in the abiotic reduction experiments. Kinetic and thermodynamic considerations indicated that neither the abundance of electron donor (lactate) nor the accumulation of aqueous end-products of oxide reduction (Fe(II), acetate, dissolved inorganic carbon) are likely to have posed significant limitations on the long-term kinetics of oxide reduction. Rather, accumulation of biogenic Fe(II) on residual oxide surfaces appeared to play a dominant role in governing the long-term kinetics of bacterial crystalline Fe(III) oxide reduction. The experimental findings together with numerical simulations support a conceptual model of bacterial Fe(III) oxide reduction kinetics that differs fundamentally from established models of abiotic Fe(III) oxide reductive dissolution, and indicate that information on Fe(III) oxide reactivity gained through abiotic reductive dissolution techniques cannot be used to predict long-term patterns of reactivity toward enzymatic reduction at circumneutral pH.

1. INTRODUCTION

Fe(III) oxides are ubiquitous components of soils and sediments, where they occur in a variety of phases ranging from poorly crystalline ferrihydrite to well-crystallized minerals such as goethite and hematite (Cornell and Schwertmann, 1996). The importance of Fe(III) oxides as electron acceptors for anaerobic respiration in Fe-rich sediments and hydromorphic soils is widely recognized (Lovley, 1991; Nealson and Saffarini, 1994), and there is significant ongoing interest in the factors that regulate the rate and extent of Fe(III) oxide reduction in such environments (Roden and Gorby, 2002). Variations in oxide particle size, surface area, and crystallinity lead to a continuum of Fe(III) oxide reactivity toward chemical dissolution (Postma, 1993). Recent studies have established that crystallographic and surface chemical (e.g., specific surface area) properties of Fe(III) oxides also exert a fundamental influence on the rate and extent of bacterial Fe(III) oxide reduction (Roden and Zachara, 1996; Roden, 2003a; Zachara et al., 1998). Available evidence suggests that oxide surface area exerts primary control on initial rates of bacterial reduction, with oxide crystal thermodynamic properties (e.g., ΔG_f, K_{sp}) playing a comparatively minor role (Fischer, 1988; Roden, 2003a). These findings indicate that Fe(III) oxide mineral heterogeneity in natural soils and sediments is likely to affect initial rates of bacterial reduction (e.g., during the early stages of anaerobic metabolism following the onset of anoxic conditions) mainly via an influence on bulk reactive surface site density.

Also of major interest in relation to the influence of oxide heterogeneity on bacterial Fe(III) oxide reduction is the degree to which changes in oxide reactivity over time influence the long-term course of reduction in permanently anaerobic sedimentary environments. A large fraction (≥ca. 80%) of amorphous Fe(III) oxide is subject to bacterial reduction in nonsulfidogenic freshwater surface sediments (Lovley and Phillips, 1986; Lovley and Phillips, 1987; Roden and Wetzel, 1996; Roden and Wetzel, 2002; Wallmann et al., 1993) and organic-contaminated shallow subsurface sediments (Heron et al., 1994; Tuccillo et al., 1999; Weiner and Lovley, 1998). In contrast, preservation of substantial quantities of crystalline Fe(III) oxides has been documented in both surface sediments (Lovley and Phillips, 1986; Phillips et al., 1993) and groundwater aquifer materials (Heron and Christensen, 1995; Roden and Urrutia, 2002; Tuccillo et al., 1999). These findings indicate that the reactivity of the Fe(III) oxide pool is likely to change significantly over time after the onset of anaerobic conditions, due to preferential dissolution of the more reactive oxide phases and/or to the accumulation of aqueous and/or surface-associated biogenic Fe(II), which down-regulates rates of bacterial crystalline Fe(III) oxide reduction at circumneutral pH (Liu et al., 2001; Roden and Zachara, 1996; Roden and Urrutia, 1999; Royer et al., 2002), through both thermodynamic and kinetic effects (Roden and Urrutia, 2002). Development of a quantitative understanding of this phenomenon is critical for construction of kinetic models of Fe(III) oxide reduction in soil and sedimentary environments.

In this study, the kinetics of bacterial and ascorbate reduction of synthetic Fe(III) oxides and natural Fe(III) oxide-bearing materials was assessed in relation to a generalized rate law for

* Author to whom correspondence should be addressed (eroden@bsc.as.ua.edu).

Table 1. Characteristics of synthetic Fe(III) oxide-coated sand and natural subsurface materials (<2 mm fraction) used in bacterial and chemical reduction experiments.

Material	Dominant Fe(III) Oxide Phase[a]	Surface Area[b] ($m^2 g^{-1}$)	CD-Fe(III)[c] (μmol g^{-1})	% HA-Ext Fe(III)[d]	% HA-Ext Fe(III)[e]	% Enzymatic Reduction[f]
Goethite-Sand	goethite	1.10 ± 0.06	105 ± 3.6	6.3 ± 0.89	2.39 ± 0.15	18.3 ± 0.4
Ferrihydrite-Sand	ferrihydrite	1.11 ± 0.31	40.7 ± 1.1	103 ± 3.3	28.3 ± 1.12	19.5 ± 3.4
HC Subsoil	goethite	20.0 ± 1.8	285 ± 19.1	1.19 ± 0.31	0.52 ± 0.04	26.1 ± 8.4
CP Subsoil	hematite	15.3 ± 1.1	197 ± 21.8	1.44 ± 0.19	0.76 ± 0.01	23.5 ± 0.8
Oyster Sediment	goethite	5.56 ± 0.58	89.1 ± 1.7	3.37 ± 0.47	1.60 ± 0.09	36.7 ± 1.2

[a] See section 2.1
[b] Multi-point BET N_2 adsorption; mean ± SD (n = 3).
[c] Citrate-Dithionite extractable Fe(III); mean ± SD (n = 3).
[d] 0.25M Ammonium Oxalate, pH 3, 4 hr extraction, expressed as percent of CD-Fe(III); mean ± SD (n = 3).
[e] 0.25M Hydroxylamine-HCl/0.25M HCl, 1 hr extraction, expressed as percent of CD-Fe(III); mean ± SD (n = 3).
[f] After 21 d (Goethite-Sand, Ferrihydrite-Sand) or 56 d (HC, CP, Oyster) incubation period (see Fig. 2), expressed as percent of CD-Fe(III); mean ± SD (n = 3).

mineral dissolution to evaluate changes in the apparent reactivity of Fe(III) oxides during long-term biologic vs. chemical reduction. The goal was to evaluate how temporal changes in oxide reactivity can be expected to influence patterns of microbial Fe(III) oxide reduction in circumneutral anoxic soils and sediments, specifically in comparison to the kinetics of bulk oxide reductive dissolution by ascorbate at pH 3. The results provide a provisional assessment of the extent to which information on Fe(III) oxide reactivity gained through chemical reduction techniques (Larsen and Postma, 2001; Postma, 1993) can be related to bacterial reduction kinetics.

2. MATERIALS AND METHODS

2.1. Oxide Phases and Characterization

The Fe(III) oxide phases employed in this study (see Table 1) included synthetic goethite- and ferrihydrite-coated sand (referred to as Gt-sand and Fh-sand, respectively) and three previously characterized Fe(III) oxide-bearing subsoil or subsurface materials (HC, CP, and Oyster). The Gt-sand was prepared by air oxidation of $FeCl_2$ in $NaHCO_3$ buffer (Schwertmann and Cornell, 1991) containing a rapidly stirred suspension (100 g L^{-1}) of quartz sand (−50 to +70 mesh; Sigma Chemicals). The Fh-sand was prepared in a similar manner by neutralization of $FeCl_3$ with 1M NaOH. The synthetic oxide-coated sands were washed free of anions by centrifugation (7000 *g* and freeze dried. The sands were then shaken briefly on a 100 μm sieve to remove small unattached oxide particles, which passed through the sieve. X-ray diffraction (XRD) analysis of goethite particles dislodged from the sand by vigorous shaking in distilled water revealed patterns consistent with goethite, and showed the broadening expected for relatively small, high-surface area particles formed during Fe(II) oxidation (Roden et al., 2000). Previous studies have demonstrated that poorly crystalline 2-line ferrihydrite is the end-product of Fh-sand synthesis using the methods employed here (Benner et al., 2002; Hansel et al., 2003).

The HC and CP materials are Fe(III) oxide/layered silicate mixtures obtained from Ultisols in Tennessee (Holston/Cloudland, Typic Fragiudult; 80–120 cm depth) and North Carolina (Cecil/Pacolet, Typic Hapludult; 40–90 cm depth), respectively. The Oyster material is Fe(III) oxide-coated sand from Pleistocene Age Atlantic Coastal Plain sediment obtained from a gravel pit in Virginia. More detailed descriptions of the properties of these materials, including information on dominant Fe(III) oxide phases as determined by XRD and/or electron microscopic imaging, are available elsewhere (Penn et al., 2001; Rai et al., 1986; Zachara et al., 1989; Zachara et al., 1995).

The natural materials were air dried and passed through a 2-mm sieve before use in experiments. The ammonium oxalate (AO)-, hydroxylamine hydrochloride (HA)-, and citrate/dithionite (CD)-extractable Fe(III) content of the synthetic and natural Fe(III) oxide-bearing materials was determined as previously described (Roden and Zachara, 1996). The surface area of the materials was determined by multi-point BET analysis (Micromeritics Model Gemini).

2.2. Bacterial Reduction Experiments

The natural Fe(III)-oxide bearing materials were autoclaved in a dry (unwetted) state every other day for three repetitions to sterilize the materials. Previous studies (Roden, unpublished data) have shown that this sterilization procedure is sufficient to prevent colonization of culture medium by sulfate-reducing bacteria present in the form of resistant spores in the air dried subsoils. The synthetic oxide coated sands were not sterilized, as previous studies have shown that no microbial growth occurs over a period of 1 month after addition of sterile medium. The synthetic and natural Fe(III) oxide bearing solids were suspended in replicate 5-mL portions of sterile anaerobic PIPES buffered (10 mM, pH 6.8) artificial groundwater medium (Roden et al., 2000) contained in sealed 10-mL serum vials to obtain a Fe(III) oxide concentration of ca. 10 mmol L^{-1}, based on the total CD-extractable Fe(III) content of the materials. The artificial groundwater medium contained 10 mM Na-lactate, 0.5 mM NH_4Cl, 0.05 mM KH_2PO_4, vitamins and trace elements, and was amended with ca. 2×10^8 cells mL^{-1} of TSB-grown *S. putrefaciens* strain CN32 cells before being combined with the oxide bearing materials. At 1–10 d intervals during a 16-d (synthetic oxide coated sand) or 56-d (natural subsurface materials) incubation period, triplicate vials were sacrificed for determination of dissolved and total (0.5M HCl-extractable) Fe(II). Dissolved Fe(II) was determined by Ferrozine analysis of small (0.1–0.5 mL) portions of particle-free unfiltered medium removed from vials in which the oxides had settled into a compact layer on the bottom of the vial. Total Fe(II) was determined by adding enough 6N HCl to the vials (following removal of samples for dissolved Fe(II)) to achieve a final concentration of 0.5M HCl (Lovley and Phillips, 1986), after which the vials were shaken (250 rpm) for 1 h before Ferrozine analysis. Vials were incubated statically at room temperature, with the exception that all vials were thoroughly mixed each time a set of three vial was sacrificed for Fe(II) analysis.

2.3. Ascorbate Reduction Experiments

A modification of the technique described by Postma (1993) was used to assess the kinetics of ascorbate reduction of synthetic oxide coated sand and natural subsurface materials. Fe(III) oxide bearing solids were suspended in 100 mL of anaerobic 10 mM ascorbic acid (pH 3) to obtain a Fe(III) oxide concentration of ca. 1 mmol L^{-1}, based on the total CD-extractable Fe(III) content of the materials (Table 1). Bottles were incubated at room temperature on a rotary shaker (250 rpm). At 0.01–10 d intervals, 1-mL samples of suspension were removed with a N_2-flushed plastic syringe and passed through a 0.2 μm syringe filter into Ferrozine.

2.4. Thermodynamic Calculations

Data from the bacterial reduction experiments were used to estimate changes in the thermodynamic favorability of Fe(III) oxide reduction as a function of measured or assumed concentrations (activities) of reactants and products. The approach taken in these calculations was analogous to that used in recent analyses by Liu et al. (2001) and Roden and Urrutia (2002) of controls on bacterial Fe(III) oxide reduction kinetics. Standard Fe(III) oxide ΔG_f values of −699, −488.6, and −742.7 for ferrihydrite ($Fe(OH)_3$), goethite (FeOOH), and hematite (Fe_2O_3), respectively (Cornell and Schwertmann, 1996) were employed in the calculations. Ferrihydrite and goethite were assumed to be the oxide phases present in the synthetic Fh-sand and Gt-sand materials, respectively. Unfortunately, there was no way to obtain independent information on the thermodynamic properties of the Fe(III) oxides present in the natural soil and sediment materials. Hence, the only alternative for thermodynamic calculations was to use standard oxide ΔG_f values for the synthetic counterparts of the dominant oxide phases identified in the natural materials (see Table 1). It is important to note in this regard that recent studies indicate that the susceptibility of natural crystalline Fe(III) oxides toward long-term bacterial reduction is equal to or less than that of their synthetic counterparts (Kukkadapu et al., 2001; Roden and Zachara, 1996; Zachara et al., 1998). Thus, use of standard ΔG_f values for well-crystallized synthetic oxides should not lead to underestimates of potential thermodynamic constraints on reduction of the natural Fe(III) oxide phases.

The MICROQL algorithm (Westall, 1986), modified to account for ionic strength effects according to the Davies equation as described in (Westall et al. (1986), was used to compute aqueous phase speciation and thereby the activities of reactant and products. Measured aqueous Fe(II) values were employed in the calculations, along with (i) estimates of lactate, acetate, and dissolved inorganic carbon (DIC) concentrations computed in accordance with appropriate stoichiometries for lactate oxidation coupled to Fe(III) oxide reduction (see Table A1); and (ii) the known composition (excluding trace elements) of the artificial groundwater medium. The lactate, acetate, and ΣDIC concentrations used in the speciation calculations were calculated based on the total amount of Fe(II) produced at a given time point, starting from baseline values of 10, 0.001, and 4.5 mM, respectively, and assuming a 1:4 ratio of lactate consumption and acetate/DIC production coupled to Fe(III) reduction. The initial DIC concentration (not measured in this study) was estimated from the pH of the buffer system (6.8) and the partial pressure of CO_2 in the N_2 gas used to deoxygenate the medium (ca. $10^{-1.5}$ atm). pH values (not measured in this study) were fixed at 6.8 for the calculations, in accordance with the very minor pH changes observed in 10 mM Pipes-buffered natural Fe(III) oxide reduction systems displaying comparable amounts of Fe(III) oxide reduction (Roden, 2003b). To assess the potential impact of small increases in pH on the thermodynamics of Fe(III) oxide reduction, an additional set of calculations was performed in which the pH was fixed at 7.2, the maximum value observed in comparable experiments on bacterial reduction of synthetic and natural Fe(III) oxides in Pipes-buffered medium with total Fe(II) production in the range of 1–10 mmol L^{-1} (Roden, unpublished data). Stability constants (log K values) for aqueous complexes were obtained from the MINEQL+ database, with the exception of those for the Fe^{2+}-CO_3^{2-}-H_2O system, which were obtained from Bruno et al. (1992). Stability constants for acetate- and lactate-metal ion complexes were obtained from Smith and Martell (1997). A log K of 2.0 was used for lactate-Fe(II) complexes, equal to the average value for several divalent cations (Smith and Martell, 1997). Listings of the components, species, and log K values employed in the speciation calculations is provided in Tables A2 and A3.

2.5. Numerical Simulations

A numerical simulation model of crystalline Fe(III) oxide reduction was developed based on the framework for computing changes in aqueous phase reactant and product concentration-speciation described above. The model is analogous to the goethite reduction models presented in Roden and Urrutia (1999) and Liu et al. (2001), in which sorption of Fe(II) to oxide surface sites is assumed to those sites unreactive toward further enzymatic reduction. Fe(II) production, together with lactate consumption and acetate/DIC production (see Eqn. 2 in Table A1), was modeled according to a fixed surface area-normalized rate of surface site reduction. To account for the influence of surface-bound Fe(II) accumulation on reactive surface site availability, a Langmuir isotherm fit to the solid-phase Fe(II) vs. aqueous Fe(II) data from the Gt-sand reduction experiment was incorporated into the equilibrium speciation routine (see Tables A2 and A3). The initial concentration of reactive surface sites was equivalent to the Γ_{max} parameter from the Langmuir isotherm fit. For simplicity, precipitation of $FeCO_3$ (s) (siderite) or $Fe_3(PO_4)_2$ (s) (vivianite) were not explicitly considered in the model, since information on the abundance of these phases was not collected. This simplification amounts to assuming that any siderite or vivianite that may have formed in the experiments was associated with residual oxide surfaces and thereby blocked reaction sites in the same manner as sorbed Fe(II). Liu et al. (2001) employed a similar assumption in simulations of synthetic goethite reduction that included siderite precipitation. The pH of the reaction system was assumed to remain constant at 6.8 in all the simulations.

The primary dependent variables and rate equations in the model are listed in Tables A4 and A5, respectively. The rate equations were integrated numerically using a fifth-order Runga-Kutta algorithm with truncation error and step size control (Press et al., 1992). Relative and absolute error tolerances were set at 0.001 (0.1%) and 10^{-12} mol L^{-1}, respectively. The equilibrium speciation routine operated within the numerical integration procedure, so that results correspond effectively (within prescribed error tolerances) to those of a fully-coupled (implicit) solution to a mixed kinetic-equilibrium speciation problem (Steefel and Macquarrie, 1996).

3. KINETIC FRAMEWORK AND INTERPRETATION

Results from the bacterial and chemical Fe(III) oxide reduction experiments were interpreted in relation to a generalized rate law for mineral dissolution (Christoffersen and Christoffersen, 1976):

$$J_t/m_0 = kf(m_t/m_0)g(C) \quad (1)$$

where J_t is the overall rate of dissolution at time t, m_0 is the initial mass (or concentration) of mineral, k is a rate constant, and m_t is the mass (or concentration) of undissolved mineral at t. The term $f(m_t/m_0)$ accounts for the influence of temporal changes in mineral crystal size, morphology, reactive site density, etc. on the rate of dissolution, whereas g(C) accounts for the influence of solution composition on dissolution rate, e.g., the case of chemical reductive dissolution, the type and concentration of reductant; or in the case of bacterial reduction, the organism(s) involved and the cell density. In situations where g(C) is known (or assumed) to be constant, the general rate law can be simplified as follows (Postma, 1993):

$$J_t/m_0 = k'(m_t/m_0)^{\gamma} \quad (2)$$

where k' is the product of the original rate constant and g(C), and the term $(m_t/m_0)^{\gamma}$ is a standard formulation for $f(m_t/m_0)$ (Christoffersen and Christoffersen, 1976; Postma, 1993). In the case of isometric crystals (e.g., spheres or cubes) that dissolve homogeneously over their entire surface area, a γ value of 2/3 is predicted from theory (Christoffersen and Christoffersen, 1976).

Postma (1993) obtained a γ value of 1.1 for reductive dissolution of synthetic ferrihydrite by ascorbic acid; the divergence of this value from the theoretical value of 2/3 can be attributed to changes in the morphology, size distribution, and reactive site density of the oxide during dissolution. Similarly, Larsen and Postma (2001) showed that nonuniformity in crystal particle size distribution and reactivity within a synthetic Fe(III) oxide mineral population can lead to γ values >2 for reductive dissolution by ascorbate. Moreover, nonuniformity of oxide particle size and reactivity within a heterogeneous mix-

ture of Fe(III) oxides, as well as temporal changes in the relative abundance of oxides with different reactivities, can lead to γ values in excess of 4 for ascorbate dissolution of Fe(III) oxides contained in natural surface and subsurface sediments (Postma, 1993). In the case of bacterial (enzymatic) Fe(III) oxide reduction, γ values will potentially reflect the influence of all the above factors, as well as the inhibitory effect of biogenic Fe(II) accumulation on enzymatic electron transfer, which is recognized as a major factor controlling the rate and long-term extent of Fe(III) oxide reduction by dissimilatory FeRB (Roden and Urrutia, 2002).

In the analysis presented below, the modified rate law (Eqn. 2) was used to assess the relative significance of the above phenomena for chemical vs. bacterial reduction of synthetic and natural Fe(III) oxide phases. The synthetic oxide-coated sands were included for comparative purposes as they were expected to display greater uniformity in reactivity relative to the natural Fe(III) oxide-bearing materials. The results of the oxide reduction experiments were fit via nonlinear least-squares regression (GraphPad Prism, Version 3.02) to the integrated form of Eqn. 2 (Larsen and Postma, 2001):

$$m_t/m_0 = [-k'(1 - \gamma)t + 1]^{1/(1-\gamma)} \quad (3)$$

4. RESULTS AND DISCUSSION

4.1. Ascorbate Reduction Kinetics

The synthetic Fe(III) oxide coated sands displayed uniform reactivity with respect to reductive dissolution by ascorbate (Fig. 1A): γ values (see Table 2) fell within the range expected for reduction of monodisperse crystal populations (Larsen and Postma, 2001; Postma, 1993). An inflection in the m_t/m_0 vs. time curve for synthetic goethite coated sand was observed at ca. 1 d, which can be attributed (based on visual observation) to dislodging of the oxide coatings from the sand, which undoubtedly increased the surface area available for reductive dissolution. The nonlinear regression analysis was therefore conducted with data from after time of oxide particle dislodgement. No such dislodging of oxide particle coatings was noted over the much shorter incubation period with ferrihydrite coated sand.

The natural Fe(III) oxide bearing materials displayed variable degrees of heterogeneity with respect to ascorbate reduction (Fig. 1B), with γ values ranging from 0.8 to 1.8 (Table 2). These values are lower than those observed by Postma (1993) for ascorbate reduction of marine surface sediment and shallow alluvial aquifer materials. One possible reason for the lower γ values is that the natural materials employed in this study contained much smaller quantities of poorly crystalline Fe(III) oxide (1.2–3.4% of total reactive Fe as estimated by AO vs. CD extraction; Table 1) compared the subsurface sediments studied by Postma (1993) (68–100% of total reactive Fe as estimated by AO versus CD extraction). Rapid, highly variable rates of dissolution of such poorly crystalline phases would be expected to lead to greater apparent heterogeneity of the bulk oxide pool with respect to ascorbate dissolution kinetics.

4.2. Bacterial Reduction Kinetics

In contrast to the relatively uniform reactivity of the synthetic and natural Fe(III) oxide bearing materials during reductive dissolution by ascorbate, these materials demonstrated

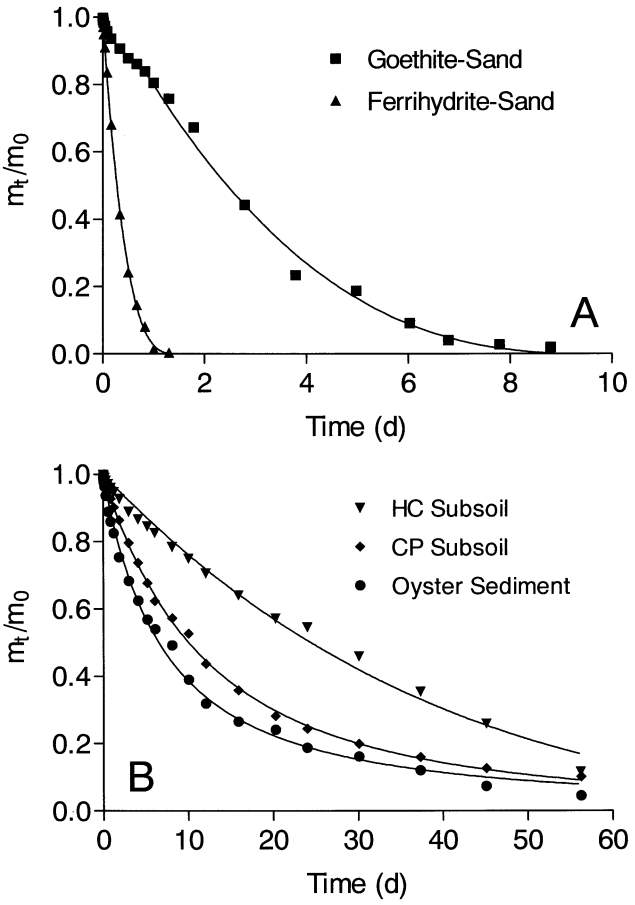

Fig. 1. Reduction of synthetic Fe(III) oxide coated sand (A) and natural Fe(III) oxide bearing materials (B) by 10 mM ascorbate at pH 3. Data are from single 100-mL suspensions. Solid lines represents nonlinear least-squares regression fits of the data to Eqn. 3 in the text.

large temporal changes in reactivity with respect to enzymatic reduction, with γ values ranging from 5.0 to 17.9 (Table 2). In all cases, m_t/m_0 values approached an asymptotic value after extended incubation (Fig. 2), and the oxides were subject to much lower degrees of overall reduction (13–39%, mean = 27.8 ± 10.5) compared to those obtained with ascorbate (90–100% mean = 94.5 ± 5.4) over the same time interval. Measurements of dissolved vs. total Fe(II) production during the bacterial reduction experiments demonstrated that a substantial fraction (28–78%) of total Fe(II) production could be accounted for by solid-phase Fe(II) accumulation (Fig. 3). Comparable patterns of Fe(III) oxide reduction aqueous:solid-phase Fe(II) partitioning have been documented in other recent pure culture experiments with natural sediments (Kukkadapu et al., 2001; Roden and Zachara, 1996; Zachara et al., 1998), as well as in shallow coastal plain aquifer materials in which the activity of indigenous FeRB was stimulated by addition of organic carbon (acetate and lactate) and inorganic nutrients (Roden and Urrutia, 2002). The dramatic deceleration and eventual cessation of bacterial Fe(III) reduction activity after only partial reduction can be attributed to the inhibitory influence of surface-bound Fe(II) accumulation on enzymatic electron transfer (e.g., via blockage of oxide surface sites; Roden and Urrutia, 1999; Roden and Urrutia, 2002) and/or thermody-

Table 2. Results of ascorbate and bacterial Fe(III) oxide reduction kinetic analyses; k′ and γ correspond to parameters in the generalized rate law for mineral dissolution (Eqn. 2 in the text).

	Ascorbate[a]			Bacterial[a]			Microbially-Reducible Fraction[b]		
Material	k′	γ	R^2	k′	γ	R^2	k′	γ	R^2
Gt-Sand	0.290 ± 0.023	0.615 ± 0.103	0.993	0.0711 ± 0.0117	17.9 ± 1.55	0.951	0.256 ± 0.055	1.65 ± 0.29	0.956
Fh-Sand	2.25 ± 0.055	0.708 ± 0.033	0.999	0.196 ± 0.040	5.77 ± 0.63	0.921	0.295 ± 0.072	1.86 ± 0.33	0.949
HC	0.0264 ± 0.0012	0.789 ± 0.097	0.992	0.0136 ± 0.0024	7.46 ± 1.46	0.857	0.0373 ± 0.0041	0.980 ± 0.191	0.97
CP	0.0824 ± 0.0015	1.50 ± 0.032	0.999	0.0415 ± 0.0039	11.8 ± 0.624	0.973	0.0888 ± 0.0018	0.927 ± 0.031	0.999
Oyster	0.140 ± 0.007	1.77 ± 0.075	0.996	0.0240 ± 0.0015	5.03 ± 0.32	0.980	0.0524 ± 0.0034	0.938 ± 0.010	0.990

[a] k′ and γ values for ascorbate and bacterial reduction are from nonlinear least-squares regression fits of the data in Figs. 1 and 2 to Eqn. 3 in the text. Error terms represent the standard error of the regression parameter.

[b] Results of nonlinear least-squares regression analysis of bacterial reduction data from which a non-reactive fraction of Fe(III) was subtracted (open symbols in Fig. 2); see section 4.2 for details.

namic constraints (see below) posed by the accumulation of aqueous reaction end-products, particularly dissolved Fe(II) (Liu et al., 2001). In the case of the Fh-sand, conversion of ferrihydrite to magnetite (see below) may also have limited the long-term degree of Fe(III) reduction (Benner et al., 2002; Fredrickson et al., 1998; Lovley and Phillips, 1986).

To assess temporal changes the apparent reactivity of the fraction of Fe(III) that was subject to enzymatic reduction (designated as the "microbially-reducible" fraction), the lowest Fe(III) concentration observed at the end of the incubation experiments was subtracted from measured Fe(III) values and the data were fit once again to Eqn. 3 (Fig. 2, open symbols). The resulting γ values were 5–10 fold lower than those esti-

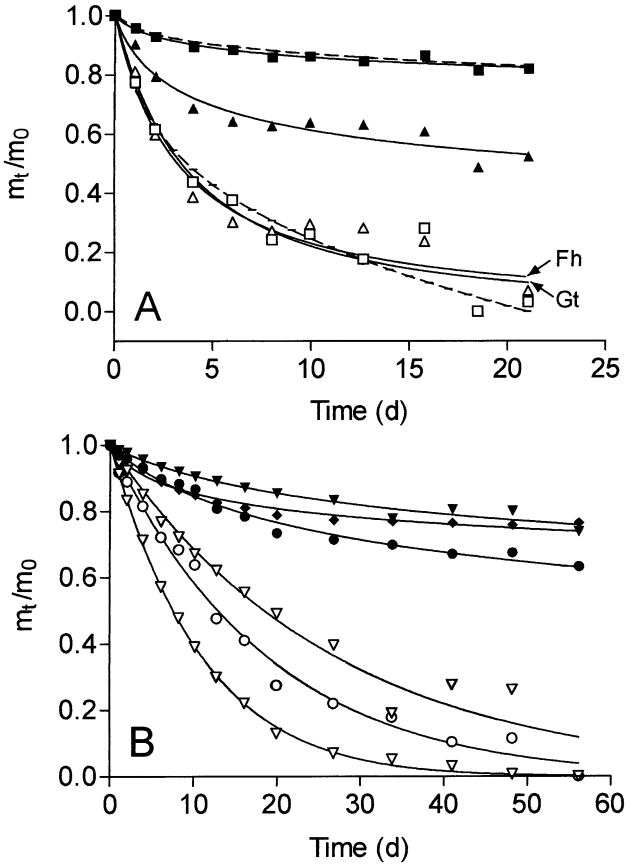

Fig. 2. Reduction of Fe(III) oxide coated sand (A) and natural Fe(III) oxide bearing materials (B) by *S. putrefaciens* strain CN32 (10^8 cells mL^{-1}, pH 6.8). Data represent the mean of triplicate cultures sacrificed at each time point. Solid symbols as in Figure 1. Open symbols represent data from which a non-reactive fraction of Fe(III) was subtracted (see 4.2 for details) Solid lines represent nonlinear least-squares regression fits of the data to Eqn. 3 in the text. Dashed lines in panel A show results of a simulation model of Gt-sand reduction (see section 4.4.2).

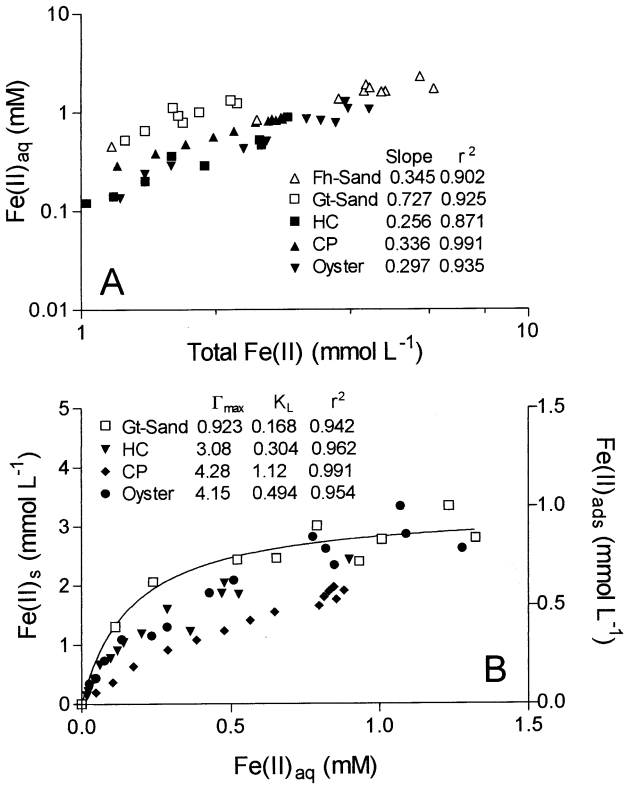

Fig. 3. Plot of aqueous Fe(II) ($Fe(II)_{aq}$) vs. total Fe(II) (A) and solid-associated Fe(II) ($Fe(II)_s$) vs. aqueous Fe(II) (B) for the bacterial reduction experiments. Data represent the mean of triplicate cultures sacrificed at each time point. Slope values in panel A legend refer to slope parameters from linear least-squares regression analyses on non-log-transformed data. Γ_{max} and K_L values in panel B legend refer to parameters from nonlinear least-squares regression fits of the data to a Langmuir isotherm ($\Gamma = \Gamma_{max}[C]/([C]+K_L)$ (Stumm, 1992). Data for Gt-sand in panel B correspond to the right-hand y-axis; the solid line shows the Langmuir isotherm fit to the Gt-sand data.

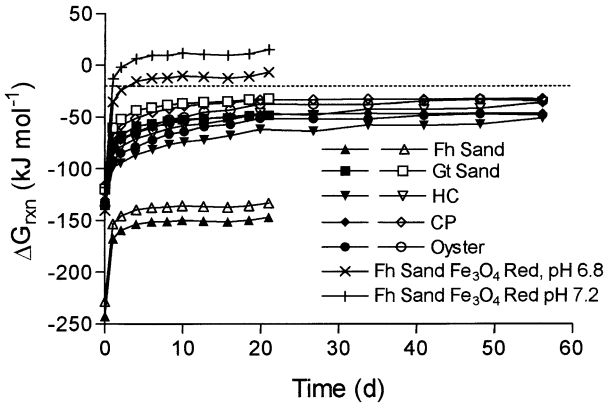

Fig. 4. Estimated changes in the thermodynamic favorability of lactate oxidation coupled to Fe(III) oxide reduction during the bacterial reduction experiments. pH values were fixed at either 6.8, the starting pH in the experiments (closed symbols); or 7.2 (open symbols), the maximum pH value observed in comparable experiments on bacterial reduction of synthetic and natural Fe(III) oxides in Pipes-buffered medium with total Fe(II) production in the range of 1–10 mmol L^{-1} (Roden, unpublished data). For Fh sand, separate calculations were performed assuming that magnetite (Fe_3O_4) was the oxide phase subject to bacterial reduction. See "Materials and Methods" and Tables A1-A3 for details of the calculations. The horizontal dashed line at a ΔG_{rxn} = –20 kJ mol^{-1} represents the theoretical minimum amount of energy required to exploit a biochemical reaction for energy conservation via ATP biosynthesis coupled to electron transport.

mated with the raw m/m_0 data (range 0.9–1.9; see Table 2), which suggests that the reducible fraction was subject to relatively uniform (pseudo first-order) enzymatic reduction kinetics (see further discussion below).

4.3. Thermodynamic Analysis

Thermodynamic calculations (see "Materials and Methods") were performed to gain insight into the relative importance of surface-bound Fe(II) accumulation compared to aqueous phase thermodynamic constraints in controlling the long-term extent of bacterial Fe(III) oxide reduction. Understanding the impact of surface site availability vs. thermodynamic effects on oxide reduction kinetics is a critical prerequisite for development of appropriate mechanistic models of enzymatic Fe(III) oxide reduction in soils and sediments. Measured aqueous Fe(II) concentrations, along with estimated changes in lactate, acetate, and DIC abundance and speciation were used to compute the free energy of lactate oxidation coupled to Fe(III) oxide reduction (referred to here as ΔG_{rxn}) according to the reaction stoichiometries listed in Table A1. The time courses of computed ΔG_{rxn} values (Fig. 4) suggest that none of the reaction systems approached conditions in which the free energy of lactate oxidation fell below -20 kJ mol^{-1}, which represents a robust estimate of the minimum free energy required to exploit a biochemical reaction for energy conservation (Schink, 1997), assuming in this case that energy conservation takes place via ATP biosynthesis coupled to electron transport, and that three protons are translocated per molecule of ATP produced (Liu et al., 2001). In addition, since the concentration of lactate in the culture medium (10 mM) was well above the K_m value for lactate catabolism by *S. putrefaciens* strain CN32 (ca. 0.5 mM; Liu et al. (2001), and ≤10% of the electron-donating equivalents in lactate were utilized during Fe(III) reduction (based on the observed maximum Fe(II) production of ca. 4 mmol Fe(II) L^{-1}, which corresponds to oxidation of only ca. 1 mM lactate), it is unlikely that kinetic limitation by electron donor concentration was important in regulating Fe(III) oxide reduction rate/extent in these experiments.

Together the above results suggest that accumulation of surface-bound Fe(II), rather than kinetic limitation by lactate abundance, or thermodynamic constraints posed by aqueous Fe(II) accumulation, is likely to have limited the long-term extent of enzymatic Fe(III) oxide reduction depicted in Figure 2. The Fh-sand system represent a special case in which bulk solid-phase conversion to magnetite (Fe_3O_4) is likely to have controlled the extent of oxide reduction, as suggested by (i) visual observation of black magnetic solids in the culture vials toward the end of the experiment; (ii) the fraction of Fe(II) in the solid-phase at the end of the experiment (0.44 ± 0.05, n = 3), which was roughly consistent with the 1:2 Fe(II):Fe(III) ratio of magnetite; and (iii) thermodynamic calculations which indicated that the free energy available for lactate oxidation coupled to magnetite reduction (made using a ΔG_f value of –1012.6 kJ mol^{-1} for magnetite (Cornell and Schwertmann, 1996) and the stoichiometry listed in Table A1) fell to values below the limiting value of –20 kJ mol^{-1} after several days of incubation (Fig. 4). The limitation on ferrihydrite reduction posed by formation of magnetite can itself be traced back to the effects of surface-bound Fe(II) accumulation, since the conversion process involves topotactic phase conversion driven by Fe(II) surface complexation (Ardizzone and Formaro, 1983; Fredrickson et al., 1998; Mann et al., 1989; Zachara et al., 2002).

4.4. Conceptual Model of Long-Term Bacterial Reduction Kinetics

4.4.1. Surface-associated Fe(II) as a fundamental regulator

The approximately first-order consumption of the microbially-reducible fraction of the synthetic and natural Fe(III) oxides demonstrated in Figure 2 (open symbols) is consistent with recent experimental and modeling studies of synthetic crystalline Fe(III) oxide (goethite and hematite) reduction (Burgos et al., 2002; Liu et al., 2001; Roden and Urrutia, 1999), in which accumulation of biogenic Fe(II) could be well-described by a rate law equivalent to Eqn. 2 with $\gamma = 1$. The pattern of Fe(II) accumulation observed in these studies was attributed to first-order consumption of a fixed number reactive surface sites, whose abundance decreased exponentially over time due to the accumulation of surface-associated Fe(II) that rendered surface sites unreactive. The results of these studies can be combined with recent findings on the reactivity of different synthetic Fe(III) oxides toward enzymatic reduction (Roden, 2003a) to produce a conceptual model that accounts for the pseudo first-order reduction of the microbially-reducible fraction of natural crystalline Fe(III) oxides evidenced in Figure 2B (open symbols). Roden (2003a) demonstrated that synthetic Fe(III) oxides with widely varying crystallinity and surface area were subject to similar initial surface area-normalized rates of reduction by *S. putrefaciens* strain CN32. If, by analogy, different natural Fe(III) oxide phases are reduced at similar surface area-specific rates, and if the accumulation of surface-bound Fe(II) exerts

primary regulation on long-term natural Fe(III) oxide reduction kinetics (as suggested by the preceding thermodynamic analysis), then a heterogeneous population of oxides in a soil or sediment might be expected to collectively display pseudo first-order reduction kinetics with respect to some operationally-defined microbially-reducible fraction of the composite oxide pool. This idea can be clarified by considering the contrast between enzymatic and ascorbate reduction kinetics. The same synthetic oxides that showed similar initial surface area-normalized rates of enzymatic reduction (7.5-fold variation that was not correlated with oxide surface area or thermodynamic properties) displayed a much wider range (86-fold) of initial ascorbate-catalyzed dissolution rates, and these rates were generally correlated with oxide surface area and thermodynamic properties (Roden, 2003a). Based on these results (and assuming that the entire Fe(III) oxide pool in a natural soil or sediment would ultimately be subject to reductive dissolution by excess ascorbate at acidic pH, i.e., no thermodynamic limitations posed by reactant consumption or end-product accumulation), one would *not* expect a natural heterogeneous oxide pool to display first-order ascorbate reduction kinetics, i.e., one would expect to obtain γ values in excess of 1.0 when fitting dissolution time course data to the generalized rate law –which is exactly what has been observed both natural and certain synthetic Fe(III) oxide populations (Larsen and Postma, 2001; Postma, 1993; this study). These considerations reinforce a conceptual model for controls on bacterial crystalline Fe(III) oxide reduction kinetics that differs fundamentally from that advanced by Postma (1993) for abiotic reductive dissolution as a result of (i) the contrasting influence of oxide surface area and crystallinity on surface area-normalized rates of enzymatic vs. abiotic reductive dissolution, together with (ii) the impact of surface-associated Fe(II) on rates of enzymatic electron transfer to residual oxide surfaces.

4.4.2. Numerical evaluation of the conceptual model

The consequences of the above conceptual model were explored quantitatively by conducting numerical experiments with a simulation model of crystalline Fe(III) oxide reduction (see section 2.5 and Tables A4 and A5). The goal was to evaluate whether or not oxide reduction data generated according to the model would conform to pseudo first-order reduction kinetics relative to an empirically-defined microbially-reducible fraction of a heterogeneous bulk oxide pool. To begin the analysis, the rate constant for oxide reduction (k_{red} in Table A5, equivalent to k' in Eqn. 2) was varied to achieve approximate agreement between observed and simulated Gt-sand reduction data (Fig. 2, dashed lines). With the calibrated model in hand, additional simulations were conducted in which the Γ_{max} parameter for Fe(II) sorption was varied randomly according to a Guassian distribution (using the gasdev algorithm in Press et al. (1992)) with mean and standard deviations equivalent to the best-fit parameters for the Gt-sand simulation. This strategy yielded a coefficient of variation (CV) value of 1.0 for the randomly varying Γ_{max} parameter. For simplicity, the best-fit K_L value for the Gt-sand experiment was used in each of the simulations. Since Γ_{max} is equivalent to the total number of oxide surface sites ($\Sigma FeOOH_{ss}$ in Tables A4 and A5), simulations with different Γ_{max} values were assumed to represent bacterial reduction of oxide phases with different reactive surface areas, which lead to differences in the long-term extent of enzymatic reduction. This assumption is consistent with the observation of marked differences in the long-term extent of bacterial reduction of synthetic goethites with varying crystallinity and surface area (Roden and Zachara, 1996). The oxide reduction rate constant was either held constant in each of the simulations (in accordance with the basic assumption of the conceptual model), or allowed to vary randomly according to a Guassian distribution with CV = 1. Ten simulations were conducted, and weighted average composite m/m_0 vs. time values were computing using a randomly-chosen mass fraction for each hypothetical goethite phase. In all of the simulations, computed ΔG_{rxn} values for FeOOH reduction coupled to lactate oxidation remained substantially more negative than the minimum value of –20 kJ mol^{-1} assumed to be required for energy conservation. The m/m_0 vs. time data for each individual simulation, as well as the composite weighted average data, were then fit to Eqn. 3. The individual and composite data transformed to account for a non-reducible fraction (equal to the individual or composite m/m_0 value at the end of the 21-d simulation period) were similarly analyzed.

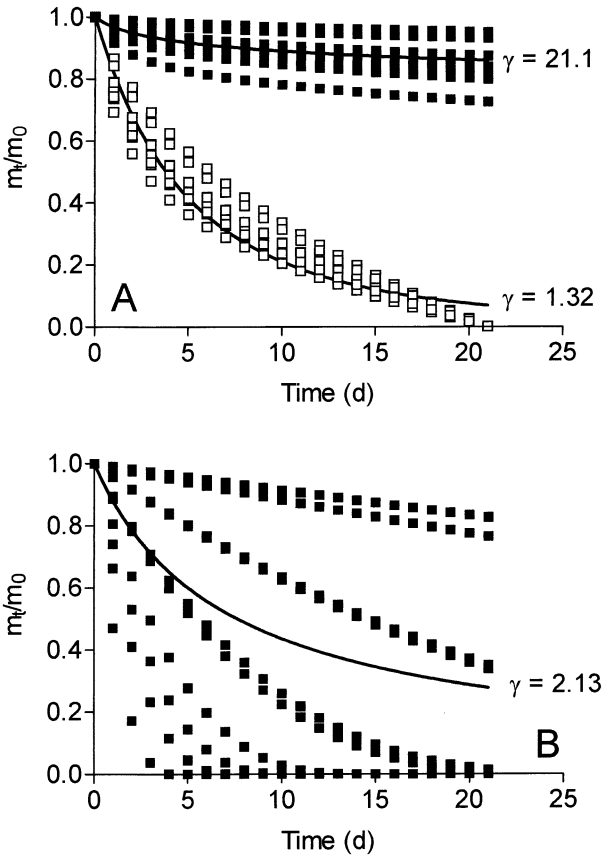

Fig. 5. Results of numerical simulations of bacterial (A) and ascorbate (B) reduction of 10 different hypothetical crystalline Fe(III) oxide phases (goethites) with varying reactive surface areas; see sections 2.5 and 4.4.2 for details. Solid symbols represent the total bulk oxide pool; open symbols in panel A correspond to the microbially-reducible (on the time scale of the simulation) fraction of the bulk pool. Solid lines show nonlinear least-squares regression fits of the composite weighted average m_t/m_0 values to Eqn. 3.

Figure 5A shows the results of the 10 simulations with fixed reduction rate constant, along with curve fits of the weighted

average composite data to Eqn. 3. The γ values obtained for the untransformed m/m_0 data ranged from 12.2 to 37.6 for the different simulations; a value of 21.1 was obtained for the weighted average composite data. In contrast, γ values for the microbially-reducible fraction ranged from 0.76 to 1.53 for the individual simulations, with a weighted average composite value of 1.32. Similar results were obtained in simulations with a variable reduction rate constants: γ values ranged from 11.3 to 31.9 and 0.84 to 1.40 for the bulk and microbially-reducible fractions, respectively, with corresponding weighted average γ values of 19.0 and 1.30. These results are in agreement with the empirical data for reduction of the natural Fe(III) oxide-bearing materials, and provide independent support for a model of natural crystalline Fe(III) reduction kinetics in which the association of biogenic Fe(II) with residual oxide surface sites leads inherently to (i) large temporal changes in apparent reactivity with respect to the bulk oxide pool; and (ii) an approximately first-order kinetic response with respect to an operationally-defined microbially-reducible fraction of the bulk oxide pool. The latter may be estimated based on long-term enzymatic reduction assays (this study), Fe(II) sorption experiments (Liu et al., 2001; Roden and Urrutia, 1999), or possibly on newly developed assays employing the reduced form of anthroquinone disulfonate (AH_2DS) at circumneutral pH (Hacherl et al., 2001).

A final illustration of the contrasting models for enzymatic vs. abiotic reductive dissolution kinetics was achieved through simulation of abiotic reductive dissolution of the 10 hypothetical oxide phases (with their associated bulk mass fractions) used in the enzymatic reduction simulations. The supposition was that the heterogeneous Fe(III) oxide pool would demonstrate, in the composite, dissolution kinetics consistent with the conceptual model advanced by Postma (1993) in which variations in mass-normalized dissolution rates among different Fe(III) oxide phases (e.g., resulting from variations in oxide crystallinity, surface area, etc.) lead to large temporal changes in the apparent reactivity of the bulk oxide pool. The mass-normalized dissolution rate constants (k' values) required for the simulations were estimated from the relationship between initial mass-normalized ascorbate reduction rate and oxide BET surface area (SA_{BET}) for the synthetic oxides studied in Roden (2003a) ($\log_{10} k' = -2.25 + 0.00640 \times SA_{BET}$, $r^2 = 0.750$, $n = 11$). Surface areas for the 10 hypothetical oxide phases were derived from the Γ_{max} parameters used in the enzymatic reduction simulations, assuming the standard mineral surface site density of 3.84 μmol m^{-1} recommended by Davis and Kent (1990). The surface area of the synthetic goethite (upon which the enzymatic reduction model was based) derived in this manner (225 m^2 g^{-1}) agreed reasonably well with the measured surface area of the oxide phase associated with the Gt-sand used in this study (186 $\pm$ 10.1 m^2 g^{-1}, determined by measuring the SA_{BET} of the Gt-sand before and after removal of the oxide coatings, and dividing the difference by the oxide mass fraction). The theoretical γ value of 2/3 for isometric crystals undergoing uniform dissolution was used in the simulations to compute instantaneous rates of oxide dissolution according to Eqn. 2. This γ value is comparable to those obtained for ascorbate dissolution of the synthetic Fh-sand and Gt-sand (Table 2). Although higher γ values have been documented for ascorbate dissolution of synthetic Fe(III) oxide phases (Larsen and Postma, 2001; Postma, 1993), the theoretical value was used in the simulations to specifically test whether or not variations in intrinsic mass-normalized dissolution rate among the different hypothetical oxide phases would generate temporal changes in composite reactivity comparable to those documented for natural Fe(III) oxides in Postma (1993) and in this study.

The simulated m/m_0 data for ascorbate dissolution of the 10 different hypothetical oxide phases are shown in Figure 5B. As expected, the wide range in mass-normalized dissolution rate constants estimated for the different oxide phases (0.00876 to 0.665; 76-fold variation) led to dramatic changes in relative rates of oxide dissolution. The γ value of 2.1 obtained from fitting the weighted average composite to Eqn. 3 is within the range thus far documented for ascorbate dissolution of natural soil/sediment Fe(III) oxide assemblages (0.8–4.7), and substantially greater than the theoretical value of 2/3 used to simulate the individual oxide phases. These results verify Postma's conceptual model for how variations in the reactivity of individual oxides –resulting from the strong influence of oxide surface and crystallographic properties on abiotic dissolution kinetics –in a heterogeneous pool can lead to large temporal changes in the apparent reactivity of the bulk pool. Interestingly, a parallel set of simulations employing a randomly varying (with CV = 1) mass-normalized reduction rate constant that was independent of oxide SA_{BET} yielded a γ value of 1.1 for the weighted average composite pool (data not shown). The similarity of this value to the γ value obtained for the microbially-reducible fraction of the composite oxide pool in the enzymatic reduction simulations ($\gamma = 1.2$; see Fig. 5A) demonstrates the general principle, embodied in the patterns of enzymatic Fe(III) oxide reduction observed in this and other recent studies (e.g., Roden and Wetzel, 2002), that the kinetics of mineral dissolution are robustly first-order with respect to some prescribed reactive fraction of the bulk pool when mass-normalized reaction rate constants are independent of the crystallographic properties of the heterogeneous mineral phases undergoing dissolution—even if the rate constants show substantial random variability about some mean value.

4.5. Quantitative Relationships Between Bacterial and Chemical Reduction Kinetics

4.5.1. Temporal changes in reactivity

Postma (1993) provided an elegant framework for comparing differences in initial mass-normalized Fe(III) oxide dissolution rates, e.g., as a function of oxide mineralogy and dissolution pathway, to temporal changes in dissolution rate during long-term chemical dissolution experiments. This framework was subsequently used by Larsen and Postma (2001) to analyze the kinetics of the bulk reductive dissolution of synthetic ferrihydrite, goethite, and lepidocrocite phases. However, a systematic evaluation of the role of microbial catalysis in relation to this framework is not yet available. The results of the studies reported here can be used to attempt an initial resolution of this issue.

The analysis is facilitated by Postma's graphical approach, in which rates of dissolution/reduction normalized to the initial oxide mass (computed using the nonlinear regression curve fits of the dissolution/reduction data shown in Figs. 1 and 2) are plotted against the fraction of oxide mass remaining (Fig. 6A).

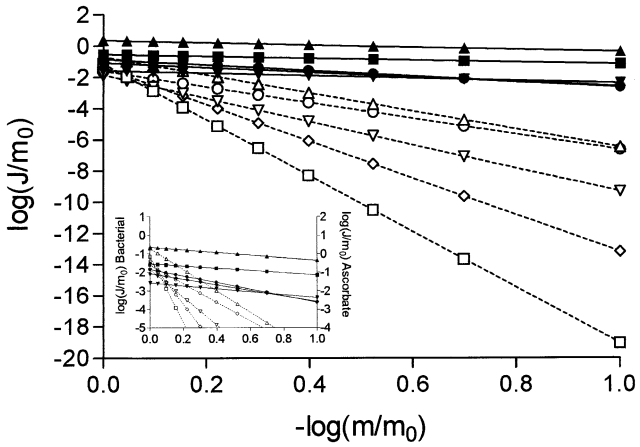

Fig. 6. Comparison of ascorbate (filled symbols) and bacterial (open symbols) Fe(III) oxide reduction rates (J, mmol Fe(III) L^{-1} d^{-1}), normalized to the initial oxide mass (m_0, mmol Fe(III) L^{-1}), as a function of the fraction of Fe(III) remaining (m/m_0). J/m_0 values for different values of m/m_0 were computed according to Eqn. 2 in the text, using parameter values listed in Table 2. Symbols as in Figures 1 and 2 (solid = ascorbate reduction; open = bacterial reduction). Inset shows expanded view of variations in initial reduction rates among the different Fe(III) oxide phases.

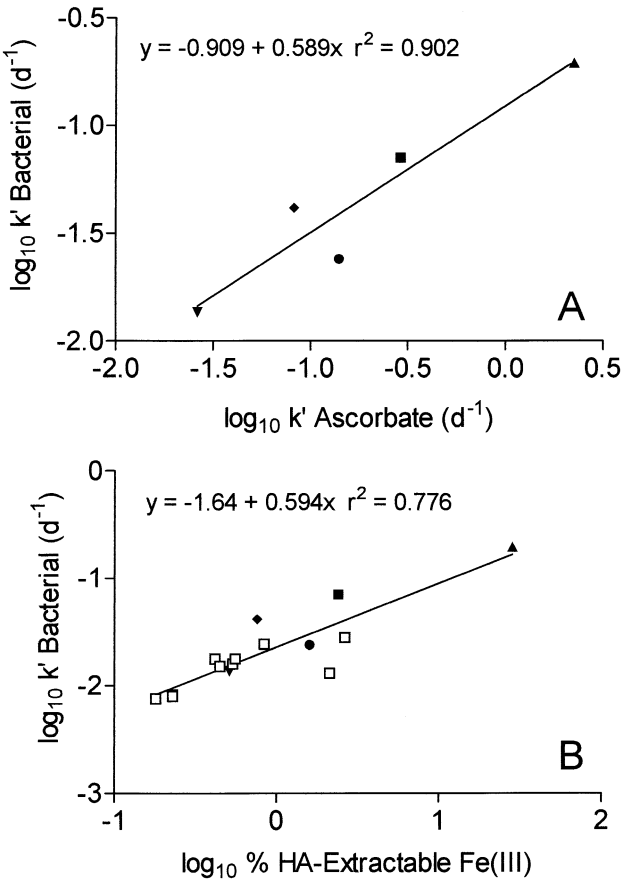

Fig. 7. Correlation between rate constants (k′ values in Table 2) for bacterial and ascorbate reduction of synthetic and natural Fe(III) oxide bearing materials (A), and between rate constants for bacterial reduction and the fraction of total Fe(III) dissolved during 1 h extraction with HA (B). Solid symbols as in Figures 1 and 2; open symbols in B are data for reduction of natural Fe(III) oxide-bearing materials inoculated with ca. 10^8 cells mL^{-1} of *S. algae* strain BrY from Roden and Zachara (1996). The solid lines show results of linear least-squares regression analyses.

Points on the y-intercept represent initial rates of reaction for the different Fe(III) oxide-bearing materials. Initial bacterial reduction rates varied by a factor of 14, whereas initial ascorbate reductive dissolution rates varied by a factor of 85. The smaller range of variation in initial bacterial reduction rates compared to ascorbate reduction rates (see Fig. 6A inset) can be attributed to the relatively uniform surface area-normalized rate of reduction across a range of oxide mineral phases, in contrast to surface area-normalized rates of ascorbate-catalyzed reduction which vary strongly with the specific surface area and thermodynamic properties of different oxide minerals (Roden, 2003a). This distinction is further illustrated by results of independent time course studies of HA-catalyzed reductive dissolution (data not shown) of the different Fe(III) oxide materials, which revealed a ca. 500-fold variation in initial dissolution rate. Collectively these results indicate that initial mass-normalized abiotic reductive dissolution rates varied by 2–3 orders of magnitude as a function of differences in oxide mineralogy, in comparison to a ca. 1 order of magnitude variation for enzymatic reduction. With respect to variation in initial reaction rates as a function of reduction pathway, enzymatic rates were 2–11 fold and 4–56 fold lower than ascorbate and HA-catalyzed rates, respectively; i.e., the range of variation was between 1 and 2 orders of magnitude. Comparison of the magnitude of these variations in initial reduction rates with temporal changes in mass-normalized enzymatic and ascorbate catalyzed reduction rates (Fig. 6) reveals the distinctive feature of enzymatic reduction discussed above, i.e., the precipitous decline in reaction rate after consumption of only a limited fraction of the total oxide pool. Calculated declines in mass-normalized enzymatic reduction rate are many orders of magnitude greater than declines in ascorbate-catalyzed rates as the degree of total reduction approaches 1.0 (i.e., as m_t/m_0 approaches zero). The predicted temporal decline in enzymatic reduction rates is also much greater than the 1–3 order of magnitude variation in initial mass-normalized reduction rates resulting from differences in oxide mineralogy and reduction pathway. These results illustrate explicitly the enormous impact which accumulation of biogenic Fe(II) has on the long-term kinetics of enzymatic Fe(III) oxide reduction at circumneutral pH.

4.5.2. *Initial rate correlations*

A significant correlation was observed between initial mass-normalized rates (k′ values in Table 2) of bacterial and ascorbate-catalyzed reduction of the synthetic and natural Fe(III) oxides (Fig. 7A). Initial rates of bacterial Fe(III) oxide reduction were similarly correlated with the fraction of total reactive Fe (CD-extractable) dissolved in a 1-h HA extraction (Fig. 7B). These results suggest that initial rates of ascorbate or HA-catalyzed Fe(III) oxide reduction may provide a proxy for rates of oxide reduction that might occur during rapid expansion of FeRB populations in subsurface environments, e.g., in situations where Fe(III) oxide reduction contributes to the oxidation of organic contaminants (e.g., land-fill leachate or petroleum hydrocarbons), or where Fe(III) reduction is stimulated for the purpose of engineered in situ remediation of metal-radionuclide

contaminants (Lovley and Anderson, 2000). However, these relationships are likely to provide crude approximations only, since FeRB cell density has a fundamental impact on bulk rates of oxide reduction (Roden and Zachara, 1996; Roden and Wetzel, 2002), and since the density of active FeRB populations in natural Fe(III)-reducing sedimentary environments—compared to the ca. 10^8 cells mL^{-1} present in the experiments depicted in Figure 6—is thus far poorly constrained (Roden and Wetzel, 2002). The abundance of FeRB cells represents a key component of the g(C) term in the generalized rate law for mineral dissolution (Eqn. 1), and quantitative analysis of the impact of this term awaits accurate determination of metabolically-active FeRB densities in natural Fe(III)-reducing sediments.

5. CONCLUSIONS AND IMPLICATIONS FOR MODELING NATURAL SOILS AND SEDIMENTS

The results of this study demonstrate that the long-term kinetics of bacterial Fe(III) oxide reduction at circumneutral pH differ significantly from those of abiotic reductive dissolution at acidic pH. Accumulation of surface-bound Fe(II) leads to progressive inhibition of enzymatic reduction, which results in large temporal changes in apparent oxide reactivity toward bacterial reduction. An key implication of these findings is that patterns of oxide reactivity observed during chemical reductive dissolution cannot be used as an indicator of the likely progress of enzymatic reduction under long-term Fe(III)-reducing conditions in natural soils and sediments. Hence, the generalized mineral dissolution rate law of Christoffersen and Christoffersen (1976), as applied to abiotic Fe(III) oxide reduction dissolution (Larsen and Postma, 2001; Postma, 1993), does not provide an accurate mechanistic representation of enzymatic Fe(III) oxide reduction activity at circumneutral pH, i.e., one suitable for numerical simulation of bacterial Fe(III) oxide reduction in soils and sediments. Although parameter estimates from nonlinear regression fits of Fe(III) reduction time course data to the generalized rate law could be employed in biogeochemical simulation models, the results would apply only to the materials under investigation, and would not be conceptually transferable to other sediment systems. Hence, recently developed modeling approaches which describe Fe(III) oxide reduction kinetics in terms of Fe(III) oxide surface site availability and thermodynamic favorability (Burgos et al., 2002; Liu et al., 2001; Roden and Urrutia, 1999; this study), which are in turn controlled by mass action relationships between sorbed and aqueous Fe(II), are likely to be more broadly useful for numerical simulation of bacterial Fe(III) oxide reduction in sediments. More detailed experimental studies of the controls on Fe(II) aqueous/solid-phase partitioning in natural Fe(III)-reducing soils and sediments, including spectroscopic (e.g., Mössbauer, XAS) analysis of the nature of Fe(II) surface speciation and its influence on surface site availability, are required to provide a rigorous mechanistic explanation for the influence of surface-bound Fe(II) on long-term bacterial reduction kinetics.

Acknowledgments—This research was supported by grants DE-FG07-ER6321 and DE-FG02–01ER63182 from the U.S. Department of Energy (DOE) Environmental Management Science Program and Natural and Accelerate Bioremediation Program, respectively. Thanks to Matilde Urrutia for review of the manuscript.

Associate editor: P. Maurice

REFERENCES

Ardizzone S. and Formaro L. (1983) Temperature induced phase transformation of metastable $Fe(OH)_3$ in the presence of ferrous ions. *Mat. Chem. Phys.* **8,** 125–133.

Benner S. G., Hansel C. M., Wielinga B. W., Barber T. M., and Fendorf S. (2002) Reductive dissolution and biomineralization of iron hydroxide under dynamic flow conditions. *Environ. Sci. Technol.* **36,** 1705–1711.

Bruno J., Wersin P., and Stumm W. (1992) On the influence of carbonate in mineral dissolution: II. The solubility of $FeCO_3$ (s) at 25 degrees C and 1 atm pressure. *Geochim. Cosmochim. Acta* **56,** 1149–1155.

Burgos W. D., Royer R. A., Fang Y., Yeh G. T., Fisher A. S., Jeon B. H., and Dempsey B. A. (2002) Theoretical and experimental considerations related to reaction-based modeling: a case study using iron(III) oxide bioreduction. *Geomicrobiol. J.* **19,** 253–292.

Christoffersen J. and Christoffersen M. R. (1976) The kinetics of dissolution of calcium sulphate dihydrate in water. *J. Crystal Growth* **35,** 79–88.

Cornell R. M. and Schwertmann U. (1996) *The Iron Oxides*. VCH.

Davis J. A. and Kent D. B. (1990) Surface complexation modeling in aqueous geochemistry. In *Mineral-water interface geochemistry* (eds. M. F. Hochella and A. F. White), pp. 177–260. Mineralogical Society of America.

Fischer W. R. (1988) Microbiological reactions of iron in soils. In *Iron in soils and clay minerals* (eds. J. W. Stucki, B. A. Goodman, and U. Schwertmann), pp. 715–748. D. Reidel Publ. Co.

Fredrickson J. K., Zachara J. M., Kennedy D. W., Dong H., Onstott T. C., Hinman N. W., and Li S. (1998) Biogenic iron mineralization accompanying the dissimilatory reduction of hydrous ferric oxide by a groundwater bacterium. *Geochim. Cosmochim. Acta* **62,** 3239–3257.

Hacherl E. L., Kosson D. S., Young L. Y., and Cowan R. W. (2001) Measurement of iron(III) bioavailability in pure iron oxide minerals and soils using anthraquinone-2,6-disulfonate oxidation. *Environ. Sci. Technol.* **35,** 4886–4893.

Hansel C. M., Benner S. G., Neiss J., Dohnalkova A., Kukkadapu R. K., and Fendort S. (2003) Secondary mineralization pathways induced by dissimilatory iron reduction of ferrihydrite under advective flow. *Geochim. Cosmochim. Acta* **67,** 2977–2992.

Heron G., Christensen T. H., and Tjell J. C. (1994) Oxidation capacity of aquifer sediments. *Environ. Sci. Technol.* **28,** 153–158.

Heron G. and Christensen T. H. (1995) Impact of sediment-bound iron on redox buffering in a landfill leachate polluted aquifer (Vejen, Denmark). *Environ. Sci. Technol.* **29,** 187–192.

Kukkadapu R. K., Zachara J. M., Smith S. C., Fredrickson J. K., and Liu C. (2001) Dissimilatory bacterial reduction of Al-substituted goethite in subsurface sediments. *Geochim. Cosmochim. Acta* **65,** 2913–2924.

Larsen O. and Postma D. (2001) Kinetics of reductive bulk dissolution of lepidocrocite, ferrihydrite, and goethite. *Geochim. Cosmochim. Acta* **65,** 1367–1379.

Liu C., Kota S., Zachara J. M., Fredrickson J. K., and Brinkman C. (2001) Kinetic analysis of the bacterial reduction of goethite. *Environ. Sci. Technol.* **35,** 2482–2490.

Lovley D. R. and Phillips E. J. P. (1986) Availability of ferric iron for microbial reduction in bottom sediments of the freshwater tidal Potomac River. *Appl. Environ. Microbiol.* **52,** 751–757.

Lovley D. R. and Phillips E. J. P. (1987) Rapid assay for microbially reducible ferric iron in aquatic sediments. *Appl. Environ. Microbiol.* **53,** 1536–1540.

Lovley D. R. (1991) Dissimilatory Fe(III) and Mn(IV) reduction. *Microbiol. Rev.* **55,** 259–287.

Lovley D. R. and Anderson R. T. (2000) The influence of dissimilatory metal reduction on the fate of organic and metal contaminants in the subsurface. *J. Hydrol.* **8,** 77–88.

Mann S., Sparks N. H. C., Couling S. B., Larcombe M. C., and Frankel R. B. (1989) Crystallochemical characterization of magnetite spinels prepared from aqueous solution. *J. Chem. Soc. Faraday Trans.* **85,** 3033–3044.

Nealson K. H. and Saffarini D. (1994) Iron and manganese in anaerobic respiration: Environmental significance, physiology, and regulation. *Annu. Rev. Microbiol.* **48,** 311–343.

Penn R. L., Zhu C., Xu H., and Veblen D. R. (2001) Iron oxide coatings on sand grains from the Atlantic coastal plain: high-resolution transmission electron microscopy characterization. *Geology* **29,** 843–846.
Phillips E. J. P., Lovley D. R., and Roden E. E. (1993) Composition of non-microbially reducible Fe(III) in aquatic sediments. *Appl. Environ. Microbiol.* **59,** 2727–2729.
Postma D. (1993) The reactivity of iron oxides in sediments: a kinetic approach. *Geochim. Cosmochim. Acta* **57,** 5027–5034.
Press W. H., Teukolsky S. A., Vetterling W. T., and Flannery B. P. (1992) Numerical Recipes in FORTRAN. Cambridge University Press.
Rai D., Zachara J. M., Ainsworth C. C., Eary L. E. and Sass B. M. (1986) Physiochemical measurements of soils at solid waste disposal sites. *Report EA-4544, Electric Power Research Institute, Palo Alto, CA.*
Roden E. E. and Wetzel R. G. (1996) Organic carbon oxidation and suppression of methane production by microbial Fe(III) oxide reduction in vegetated and unvegetated freshwater wetland sediments. *Limnol. Oceanogr.* **41,** 1733–1748.
Roden E. E. and Zachara J. M. (1996) Microbial reduction of crystalline iron(III) oxides: Influence of oxide surface area and potential for cell growth. *Environ. Sci. Technol.* **30,** 1618–1628.
Roden E. E. and Urrutia M. M. (1999) Ferrous iron removal promotes microbial reduction of crystalline iron(III) oxides. *Environ. Sci. Technol.* **33,** 1847–1853.
Roden E. E., Urrutia M. M., and Mann C. J. (2000) Bacterial reductive dissolution of crystalline Fe(III) oxide in continuous-flow column reactors. *Appl. Environ. Microbiol.* **66,** 1062–1065.
Roden E. E. and Gorby Y. A. (2002) Introduction to special issue on microbial Fe(III) oxide reduction. *Geomicrobiol. J.* **19,** 139–140.
Roden E. E. and Urrutia M. M. (2002) Influence of biogenic Fe(II) on bacterial reduction of crystalline Fe(III) oxides. *Geomicrobiol. J.* **19,** 209–251.
Roden E. E. and Wetzel R. G. (2002) Kinetics of microbial Fe(III) oxide reduction in freshwater wetland sediments. *Limnol. Oceanogr.* **47,** 198–211.
Roden E. E. (2003a) Fe(III) oxide reactivity toward biological versus chemical reduction. *Environ. Sci. Technol.* **37,** 1319–1324.
Roden E. E. (2003b) Diversion of electron flow from methanogenesis to crystalline Fe(III) oxide reduction in acetate-limited cultures of wetland sediment microorganisms. *Appl. Environ. Microbiol.* **69,** 5702–5706.
Royer R. A., Burgos W. D., Fisher A. S., Unz R. F., and Dempsey B. A. (2002) Enhancement of biological reduction of hematite by electron shuttling and Fe(II) complexation. *Environ. Sci. Technol.* **36,** 1939–1946.
Schink B. (1997) Energetics of syntrophic cooperation in methanogenic degradation. *Microbiol. Mol. Biol. Rev.* **61,** 262–280.
Schwertmann U. and Cornell R. M. (1991) *Iron Oxides in the Laboratory*. Weinheim.
Smith R. M, Martell A. E (1997) NIST Critically Selected Stability Constants of Metal Complexes Database. Version 3.0 User's Guide and Database Software. *NIST Standard Reference Database*. 46.
Steefel C. I. and MacQuarrie K. T. B. (1996) Approaches to modeling of reactive transport in porous media. In *Reactive transport in porous media*, Vol. 34 (eds. P. C. Lichtner, C. I. Steefel, and E. H. Oelkers), pp. 83–129. The Mineralogical Society of America.
Stumm W. (1992) *Chemistry of the solid-water interface*. John Wiley & Sons.
Tuccillo M. E., Cozzarelli I. M., and Herman J. S. (1999) Iron reduction in the sediments of a hydrocarbon-contaminated aquifer. *Appl. Geochem.* **14,** 655–667.
Wallmann K., Hennies K., Konig I., Petersen W., and Knauth H. D. (1993) New procedure for determining reactive Fe(III) and Fe(II) minerals in sediments. *Limnol. Oceanogr.* **38,** 1803–1812.
Weiner J. M. and Lovley D. R. (1998) Anaerobic benzene degradation in petroleum-contaminated aquifer sediments after inoculation with a benzene-oxidizing enrichment. *Appl. Environ. Microbiol.* **64,** 775–778.
Westall J. C (1986) MICROQL I. A chemical equilibrium program in BASIC. *Report*., 86–02:Department of Chemistry, Oregon State University, Corvalis, OR.
Westall J. C., Zachary J. L. and Morel F. M. M.(1986) MINEQL. A computer program for the calculation of the chemical equilibrium composition of aqueous systems. *Report*., 86–01:Department of Chemistry, Oregon State University, Corvalis, OR.
Zachara J. M., Ainsworth C. C., Cowan C. E., and Resch C. T. (1989) Adsorption of chromate by subsurface soil horizons. *Soil Sci. Soc. Am. J.* **53,** 418–428.
Zachara J. M., Smith S. C., and Kuzel L. S. (1995) Adsorption and dissociation of Co-EDTA complexes in Fe oxide containing subsurface soils. *Geochim. Cosmochim. Acta* **59,** 4825–4844.
Zachara J. M., Fredrickson J. K., Li S. W., Kennedy D. W., Smith S. C., and Gassman P. L. (1998) Bacterial reduction of crystalline Fe(III) oxides in single phase suspensions and subsurface materials. *Am. Mineral.* **83,** 1426–1443.
Zachara J. M., Kukkadapu R. K., Fredrickson J. K., Gorby Y. A., and Smith S. C. (2002) Biomineralization of poorly crystalline Fe(III) oxides by dissimilatory metal reducing bacteria (DMRB). *Geomicrobiol. J.* **19,** 179–207.

APPENDIX

Table A1. Stoichiometries for lactate oxidation coupled to the reduction of ferrihydrite, goethite, hematite, and magnetite. The stoichiometries were used in conjunction with measured or estimated concentrations/activities of reactants and products to generate the thermodynamic calculations shown in Fig. 4.

1. Ferrihydrite reduction
$4Fe(OH)_3 + CH_3CHOHCOO^- + 7H^+ \rightarrow 4Fe^{2+} + CH_3COO^- + HCO_3^- + 10H_2O$
2. Goethite reduction
$4FeOOH + CH_3CHOHCOO^- + 7H^+ \rightarrow 4Fe^{2+} + CH_3COO^- + HCO_3^- + 6H_2O$
3. Hematite reduction
$2Fe_2O_3 + CH_3CHOHCOO^- + 7H^+ \rightarrow 4Fe^{2+} + CH_3COO^- + HCO_3^- + 4H_2O$
4. Magnetite reduction
$2Fe_3O_4 + CH_3CHOHCOO^- + 11H^+ \rightarrow 6Fe^{2+} + CH_3COO^- + HCO_3^- + 6H_2O$

Table A2. Components in equilibrium speciation system.

Component	Initial total concentration (mol L^{-1})[a]
$CH_3CH_2OHCOO^-$ (lactate)	1.00×10^{-2}
CH_3COO^- (acetate)	1.00×10^{-6}
Ca^{2+}	6.13×10^{-4}
Cl^-	2.02×10^{-3}
CO_3^{2-}	4.50×10^{-3}
Fe^{2+}	1.00×10^{-6}
H^+	1.02×10^{-2}
K^+	2.51×10^{-4}
Mg^{2+}	2.46×10^{-4}
NH_4^+	5.00×10^{-4}
Na^+	2.50×10^{-2}
$Pipes^-$	1.00×10^{-2}
PO_4^{3-}	5.00×10^{-5}
$FeOOH_{fss}$	9.90×10^{-4}

[a] Initial H^+ concentration corresponds to TOTH; initial $FeOOH_{fss}$ corresponds to bulk surface site density derived from Langmuir fits to solid-phase Fe(II) vs. aqueous Fe(II) data for the Gt-sand reduction experiment (Fig. 3B). The $FeOOH_{fss}$ component and associated adsorbed Fe(II) species ($Fe(II)_{ads}$; see Table A3) were included only in the goethite simulation model described in sections 2.5 and 4.4.2.

Table A3. Aqueous and sorbed species and associated equilibrium mass action equations.

Reaction			log K
$[CH_3COO]$	=	$[CH_3COO^-]\,[H^+]$	4.76
$[CaOH^+]$	=	$[Ca^{2+}]\,[H^+]^{-1}$	−12.6
$[CaCH_3COO^+]$	=	$[Ca^{2+}]\,[CH_3COO^-]$	1.18
$[CaHCO_3^+]$	=	$[Ca^{2+}]\,[CO_3^{2-}]\,[H^+]$	11.33
$[CaCO_3(aq)]$	=	$[Ca^{2+}]\,[CO_3^{2-}]$	3.15
$[CaCH_3CH_2OHCOO^+]$	=	$[Ca^{2+}]\,[CH_3CH_2OHCOO^-]$	1.45
$[CaHPO_4(aq)]$	=	$[Ca^{2+}]\,[PO_4^{3-}]\,[H^+]$	15.09
$[H_2CO_3]$	=	$[CO_3^{2-}]\,[H^+]^2$	16.68
$[HCO_3]$	=	$[CO_3^{2-}]\,[H^+]$	10.33
$[FeOH^+]$	=	$[Fe^{2+}]\,[H^+]^{-1}$	−9.5
$[FeCH_3COO^+]$	=	$[Fe^{2+}]\,[CH_3COO^-]$	1.82
$[FeHCO_3^+]$	=	$[Fe^{2+}]\,[CO_3^{2-}]\,[H^+]$	12.33
$[FeCO_3(aq)]$	=	$[Fe^{2+}]\,[CO_3^{2-}]$	5.50
$[Fe(CO_3)_2^{2-}]$	=	$[Fe^{2+}]\,[CO_2]^2$	7.10
$[FeCH_3CH_2OHCOO^+]$	=	$[Fe^{2+}]\,[CH_3CH_2OHCOO^-]$	2.00
$[FeH_2PO_4^+]$	=	$[Fe^{2+}]\,[PO_4^{3-}]\,[H^+]^2$	22.50
$[FeCl^+]$	=	$[Fe^{2+}]\,[Cl^-]$	0.90
$[KHPO_4]$	=	$[K^+]\,[PO_4^{3-}]\,[H^+]$	12.60
$[CH_3CH_2OHCOO^+]$	=	$[CH_3CH_2OHCOO^-]\,[H^+]$	3.86
$[MgOH^+]$	=	$[Mg^{2+}]\,[H^+]^{-1}$	−11.79
$[MgCH_3COO^+]$	=	$[Mg^{2+}]\,[CH_3COO^-]$	1.14
$[MgHCO_3^+]$	=	$[Mg^{2+}]\,[CO_3^{2-}]\,[H^+]$	11.40
$[MgCO_3(aq)]$	=	$[Mg^{2+}]\,[CO_3^{2-}]$	2.98
$[MgCH_3CH_2OHCOO^+]$	=	$[Mg^{2+}]\,[CH_3CH_2OHCOO^-]$	1.37
$[MgHPO_4^+]$	=	$[Mg^{2+}]\,[PO_4^{3-}]\,[H^+]$	15.22
$[NaCH_3COO(aq)]$	=	$[Na^+]\,[CH_3COO^-]$	−0.18
$[NaHCO_3]$	=	$[Na^+]\,[CO_3^{2-}]\,[H^+]$	10.08
$[NaCO_3^-]$	=	$[Na^+]\,[CO_3^{2-}]$	1.27
$[NH_3(aq)]$	=	$[NH_4^+]\,[H^+]^{-1}$	−9.25
[HPipes]	=	$[Pipes^-]\,[H^+]$	6.70
$[HPO_4^{2-}]$	=	$[PO_4^{3-}]\,[H^+]$	12.35
$[H_2PO_4^-]$	=	$[PO_4^{3-}]\,[H^+]^2$	19.55
$[H_3PO_4(aq)]$	=	$[PO_4^{3-}]\,[H^+]^3$	21.71
$[Fe(II)_{ads}]$	=	$[FeOOH_{fss}]\,[Fe^{2+}]$	4.30[a]
$[OH^-]$	=	$[H^+]^{-1}$	−14.00

[a] Derived from Langmuir isotherm fits to solid-phase Fe(II) vs. aqueous Fe(II) data for the Gt-sand reduction experiment (Fig. 3B), accounting for aqueous equilibrium speciation effects.

Table A4. Dependent variables in goethite reduction simulation model.

Variable[a]	Initial value (mol L^{-1})
$\Sigma FeOOH_{ss}$ ($FeOOH_{fss}$ + $Fe(II)_{ads}$)	9.90×10^{-4}
$\Sigma CH_3CH_2OHCOO^-$ (lactate)	1.00×10^{-2}
$\Sigma Fe(II)$ ($Fe(II)_{aq}$ + $Fe(II)_{ads}$)	1.00×10^{-6}
ΣCH_3COO^- (acetate)	1.00×10^{-6}
ΣCO_3^{2-}	4.50×10^{-2}
ΣH^+ (TOTH)	1.02×10^{-2}

[a] Σ indicates total of all aqueous (and sorbed) species associated with a component involved in equilibrium speciation reactions (see Table A3).

Table A5. Rate expressions for kinetic reactions in the goethite reduction simulation model.

Reaction	Rate Expression
FeOOH reduction	$R_{FeOOH} = -k_{red}\,[FeOOH_{fss}]$ where $[FeOOH_{fss}] = [\Sigma FeOOH_{ss}] - [Fe(II)_{ads}]$
Lactate consumption	$R_{Lactate} = -0.25R_{FeOOH}$
Fe(II) production	$R_{\Sigma Fe(II)} = R_{FeOOH}$
DIC production	$R_{\Sigma CO3} = 0.25R_{FeOOH}$
Acetate production	$R_{Acetate} = 0.25R_{FeOOH}$
TOTH production/ consumption[a]	$R_{TOTH} = -2R_{FeOH}$

[a] Although changes in TOTH were computed in the model, the pH of the medium was assumed to be fixed at 6.8 for the simulations presented in this paper.